Bifurcation of dividing surfaces constructed from a pitchfork bifurcation of periodic orbits in a symmetric potential energy surface with a post-transition-state bifurcation

Matthaios Katsanikas,[1, *] Makrina Agaoglou,[2, †] and Stephen Wiggins[1, ‡]

[1]*School of Mathematics, University of Bristol,*
Fry Building, Woodland Road, Bristol, BS8 1UG, United Kingdom.
[2]*Instituto de Ciencias Matemáticas, CSIC, C/Nicolás Cabrera 15, Campus Cantoblanco, 28049 Madrid, Spain*

In this work we analyze the bifurcation of dividing surfaces that occurs as a result of a pitchfork bifurcation of periodic orbits in a two degrees of freedom Hamiltonian System. The potential energy surface of the system that we consider has four critical points:two minima, a high energy saddle and a lower energy saddle separating two wells (minima). In this paper we study the structure, the range, and the minimum and maximum extent of the periodic orbit dividing surfaces of the family of periodic orbits of the lower saddle as a function of the total energy.

I. INTRODUCTION

The aim of this paper is to study a bifurcation of periodic orbit dividing surfaces that occurs as a result of a pitchfork bifurcation of periodic orbits. For this reason we choose a pitchfork bifurcation of periodic orbits that takes place in a Hamiltonian system with two degrees of freedom. The potential energy surface (PES) that we use is symmetric about the x-axis and it has four critical points: two index-1 saddles and two minima. One index-1 saddle (the upper index-1 saddle) has higher energy than the other index-1 saddle (the lower index-1 saddle) and the lower index-1 saddle separates the two potential wells (the upper well and the lower well). Between the two index-1 saddles is a valley ridge inflection (VRI) point, where the shape of the potential near the VRI point changes from a valley to a ridge. This potential has been studied recently ([1–7]).

Dividing surfaces are surfaces of one less dimension than that of the potential energy surface. These surfaces are important for the Transition State Theory (TST) (see [8, 9]) in chemical reaction dynamics. In Hamiltonian systems with two degrees of freedom, the periodic orbit dividing surfaces are 2-dimensional surfaces in the energy surface. The construction of the periodic orbit dividing surfaces is constructed through the classical method of [10–14] in Hamiltonian systems with two degrees of freedom. The construction of the periodic orbit dividing surfaces in Hamiltonian with three or more degrees of freedom can be done through the method of [15, 16].

An invariant, closed, oriented, co-dimension-2 submanifold of an energy level that can be spanned by two compact codimension-1 submanifolds of unidirectional flux whose union, a dividing surface, separates locally the energy level into two components and it has no local recrossing is called a transition state (see [17]). The bifurcations of transition states (unstable periodic orbits and NHIMs) in chemical reaction dynamics have been used in order to understand: A) The breakdown of transition state theory in collinear $HgI_2 \rightarrow HgI + I$ reaction [18] and the hydrogen exchange reaction (see [19]). B) The influence of no-return transition states in the reaction rate of hydrogen exchange reaction [20]. C) The loss and regain of normal hyperbolicity of the transition states in a three-dimensional Hamiltonian model of the hydrogen exchange reaction [21]. D) The bridge between reactant and product channels in the collinear FH_2 reactive system [22]. E) The study of systems in which as the energy varies the transition state becomes singular and then regains the normal hyperbolicity with a change in differentiability as described through Morse bifurcations (see [17]). F) The separation of reactants and products and the flux through the dividing surface (see [23]). G) The transport of trajectories from the region of the higher index-1 saddle to the region of the top and bottom well in a symmetric potential energy surface with a post-transition-state bifurcation through a pitchfork bifurcation (see [2, 3]).

The basic and initial motivation of this work is to continue our previous work ([2, 3]) by investigating the effects of a pitchfork bifurcation on the structure of the dividing surfaces of the top and bottom unstable periodic orbits (that bifurcate from the family of the lower saddle through a pitchfork bifurcation) that are responsible for the transport of the trajectories from the region of the higher index-1 saddle to the region of the top and bottom well (see [2, 3]). In all the papers that were mentioned in the previous paragraph except ([17],[23]), the studies were focused on the applications of the bifurcations of periodic orbits (see [24] for a review of the many types of bifurcations in Hamiltonian

---

* matthaios.katsanikas@bristol.ac.uk

† makrina.agaoglou@icmat.es

‡ s.wiggins@bristol.ac.uk

systems with two and three degrees of freedom in chemical reaction dynamics) and NHIMs in different settings of chemical reactions, but they did not focus on the effects of these bifurcations on the structure and geometry of dividing surfaces. In this paper, we deal with this problem and in particular with the evolution of the geometry of dividing surfaces as the energy increases and the family of periodic orbits of the lower saddle undergoes a pitchfork bifurcation in a symmetric potential energy surface with a post-transition-state bifurcation ([2, 3]). These surfaces are spheres or ellipsoids before and after a bifurcation, as is also shown for integrable cases of Hamiltonian systems [23]). They are presented as disks in the 3D projection (x, y, p_x) of the phase space, before and after a pitchfork bifurcation in a non-integrable Hamiltonian system with two degrees of freedom ([25]). In our case, we will study in a more systematic way the change of the geometry of the dividing surfaces, before and after a pitchfork bifurcation, investigating the structure of the dividing surfaces in all 3D projections of the phase space of a non-integrable Hamiltonian system with two degrees of freedom. We will also describe in detail the structure of the dividing surfaces in a system in which the structure of dividing surfaces is more complicated (the dividing surfaces are initially not disks in the 3D projection (x, y, p_x) but filamentary structures) than that of the dividing surfaces that are found in the Hamiltonian model of [25]. Furthermore, we will follow the complex distortion of these surfaces that are initially ellipsoids or filamentary structures in the 3D projections of the phase space as we change the energy. We emphasize the fact that we investigated the distortion of the dividing surfaces (that are initially ellipsoids or filamentary structures) through a pitchfork bifurcation of periodic orbits, and not situations where the dividing surfaces change topology and become tori or other topological structures though a Morse bifurcation (see [17]). The study of topological changes of this kind (through a Morse bifurcation) is an interesting topic but out of the scope of this paper. We study, also the evolution of other geometrical characteristics, such as the range and the maximum and minimum value of the dividing surfaces.

We describe the PES of our system in section II. We describe the pitchfork bifurcation of periodic orbits of the lower saddle in section III. Then in section IV, we describe our results about the structure of the diving surfaces. Finally, we discuss our results and we present our conclusions in the last section V.

II. MODEL

The analytical form of the PES that was inspired by [1] is the following:

$$V(x, y) = \frac{8x^3}{3} - 4x^2 + \frac{y^2}{2} + xy^2(y^2 - 2). \tag{1}$$

The PES has an upper index-1 saddle (exit/entrance channel) and a lower index-1 saddle, which is an energy barrier separating two potential wells. Moreover, the PES is symmetric about the x axis. A three dimensional plot of the PES is given in Fig. II. The two dimensional (2D) Hamiltonian is given by

$$H(x, y, p_x, p_y) = \frac{p_x^2}{2} + \frac{p_y^2}{2} + V(x, y), \tag{2}$$

and the corresponding Hamiltonian vector field (i.e. Hamilton's equations of motion) is:

$$\begin{cases} \dot{x} = p_x, \\ \dot{y} = p_y, \\ \dot{p}_x = 8x(1 - x) + y^2(2 - y^2), \\ \dot{p}_y = y\left(4x(1 - y^2) - 1\right). \end{cases} \tag{3}$$

Hamilton's equations conserve the total energy, which we will denote as E throughout the text.

III. PERIODIC ORBITS

In this section, we present a pitchfork bifurcation of the family of the lower saddle. As we explained in the previous section, we have two index-1 saddles, one for higher values of energy and one for lower values of energy. According to the Lyapunov subcenter theorem we have a family of periodic orbits associated with every index-1 saddle (see [26–28]). In this section we follow the family of periodic orbits associated with the lower index-1 saddle, increasing
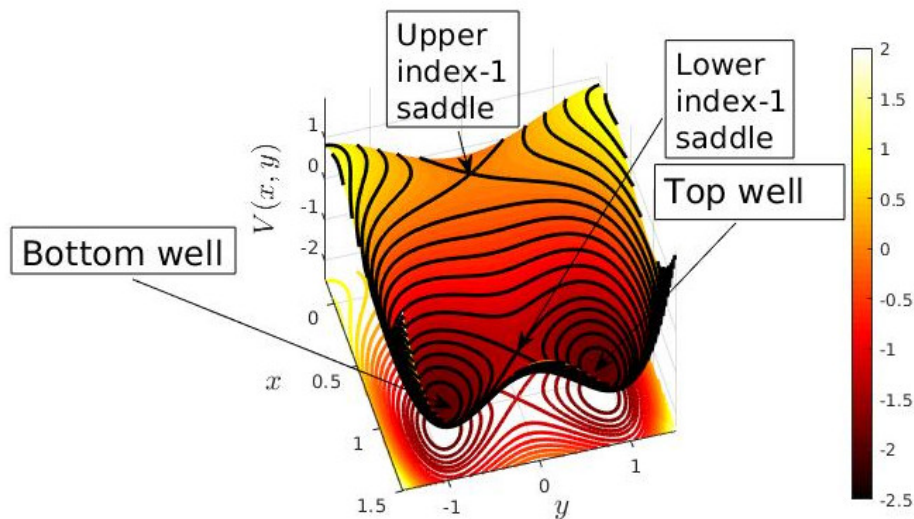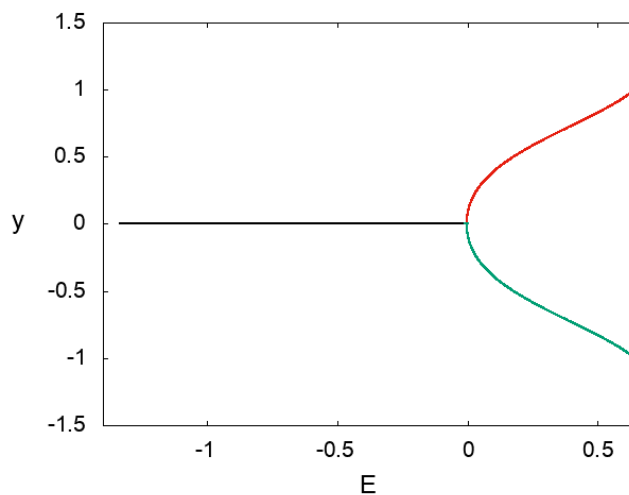
Figure 1. Plot of the PES given in Eq. (1).

Figure 2. The evolution of the coordinate y of periodic orbits on the Poincaré section $x = 0.05$ versus energy (characteristic diagram). The family of periodic orbits of the lower saddle is depicted by black color and its bifurcating families, the families of the top and bottom unstable periodic orbits, are depicted by red and green color, respectively.

the energy above the energy of the lower index-1 saddle. The periodic orbits of this family lie on the x-axis (see Fig. 8).

In the characteristic diagram (a diagram that shows the evolution of a coordinate of periodic orbits of a family in a Poincaré section versus the energy of the system - see Fig. 2) we see that the family of periodic orbits associated with the lower saddle undergoes a pitchfork bifurcation at $E = -0.00056$. At this value the family of periodic orbits associated with the lower index-1 saddles, that was initially unstable, becomes stable. At this point we have two new unstable families of periodic orbits which we refer to as the top and bottom families of periodic orbits (see more details for the role of the these periodic orbits in the dynamics of the system in [2, 3, 5, 6]). We observe, in Figs. 9, 10, that by increasing the energy the periodic orbits of these families become more elongated in the direction of the y-axis. In these figures we see that the POs of the top and bottom families are converging to the line $y = 0$ from above and below, respectively.

IV. RESULTS

Initially (for values of energy above the energy of the lower saddle, $E = -4/3$ and before the pitchfork bifurcation for $E = -0.00056$) we have the family of periodic orbits of the lower saddle that gives rise to a family of dividing surfaces. For the construction of the periodic orbit dividing surfaces we use he classical algorithm of [10, 11, 13, 14, 29], that is presented in our previous papers (see ([6, 30]). After the pitchfork bifurcation of the periodic orbits of the family of the lower saddles (see the previous section) we have two new bifurcating families, the top and bottom unstable periodic orbits. These families give rise to two new families of dividing surfaces. In this section, we study the evolution of the structure and the range and of the minimum and maximum of the dividing surfaces that are constructed from the periodic orbits of the lower saddle and its bifurcations as energy is varied:

1. **The structure of the dividing surfaces:** The periodic orbit dividing surfaces that are constructed from the periodic orbits of the lower saddles are presented as ellipsoids in the (x, p_x, p_y) projection (see Fig. 3). This ellipsoid becomes more stretched and sharp as we increase the energy (see the 2D projections (x, p_x) of the dividing surfaces in Fig. 11). Furthermore, these dividing surfaces are presented as filamentary structures, that lie on the plane $y = 0$, in the (x, y, p_x) and (x, y, p_y) subspaces of the phase space (see panel B of Fig. 3 and panel A of Fig. 5) and in the (y, p_x, p_y) subspace of the phase space (see panel B of Fig. 5). This filamentary structure of these surfaces is because of the morphology of the periodic orbits of the lower saddles in the configuration space (it lies on the line $y = 0$ - see the previous section). This is the reason that the 2D projections (y, p_y) of the dividing surfaces of the family of lower saddle (Fig. 14) is the line $y = 0$ for all energies.

   As the energy is increased above that of the pitchfork bifurcation, in addition to the dividing surfaces of the family of the lower saddles, we have two other families of dividing surfaces. One family corresponds to the dividing surfaces of the top unstable periodic orbits and the other to the dividing surfaces of the bottom unstable periodic orbits. The dividing surfaces of these families are on both sides of the dividing surfaces of the family corresponding to the lower saddles in the 3D projections (x, y, p_x), (x, y, p_y) and (y, p_x, p_y) (see panels C and D of Fig. 5). The dividing surfaces of the bifurcating families in the 3D projections, (x, y, p_x) and (x, y, p_y), are presented as filamentary structures that are curved in the direction of positive y-values (the dividing surfaces of the top unstable periodic orbits) or on the direction of negative y-values (the dividing surfaces of the bottom unstable periodic orbits). The structure of these dividing surfaces in the 3D subspace (y, p_x, p_y) is similar to that of an ellipsoid that is a little sharper in one direction (see for example Fig. 4). In addition, the dividing surfaces of the family of the lower saddle coincide with the dividing surfaces of the two bifurcating families in the (x, p_x, p_y) subspace of the phase space and they have the same structure (an ellipsoid) as that of panel A of Fig. 3.

   For values of energy larger than 0 (the energy of the upper saddle) the family of periodic orbits of the lower saddle vanishes. Consequently, the family of dividing surface of the lower saddle vanishes too. This means that the dividing surfaces of the family of the lower saddle do not exist between the dividing surfaces of the bifurcating families in the 3D projections (x, y, p_x), (x, y, p_y) and (y, p_x, p_y) (see the panels E and F of Fig. 5). We notice also that the distance between the dividing surfaces of the top and bottom unstable periodic orbits, in the 3D projections (x, y, p_x), (x, y, p_y) and (y, p_x, p_y), increases as the energy increases (compare the panels C and D of Fig. 5 with the panels E and F of Fig. 5).

   As we increase the energy, the dividing surfaces of the bifurcating families in the 3D subspace (x, p_x, p_y) become more round/ellipsoidal as the energy increases (see the 2D projections (x, p_x) of the dividing surfaces of the top and bottom unstable periodic orbits in Figs. 12, 13). Furthermore, we observe a decrease of the sharpness of the ellipsoidal dividing surfaces of the bifurcating families in the 3D subspace (y, p_x, p_y), as we increase the energy (see the 2D projections (y, p_y) of the dividing surfaces of the top and bottom unstable periodic orbits in Figs. 15, 16).

2. **Maximum and Minimum of the dividing surfaces:** In Fig. 6 we present in the left column the minimum of the dividing surfaces with respect to the x coordinate, y coordinate and p_x coordinate (panels A, C and E respectively) of the family of the lower saddle (black line), top family (red line) and bottom family (green line), respectively. Similarly, in the right column of the figure we show the maximum of the dividing surfaces with respect to the x coordinate, y coordinate and p_x coordinate (panels B, D and F respectively) of the family of the lower saddle (black line), top family (red line) and bottom family (green line), respectively. Note that we did not show the minimum and maximum of p_y coordinate because it is determined from the other three coordinates through the Hamiltonian of the system. We observe that in the panel A the minimum of the family of the lower saddle is decreasing as the energy increases, as does does the minimum of the top and bottom families so that they coincide. In the panels B, E and F we notice that there is a continuation of the minima and maxima of the family of the lower saddle to the other two bifurcating families (they coincide with each other). Finally in the
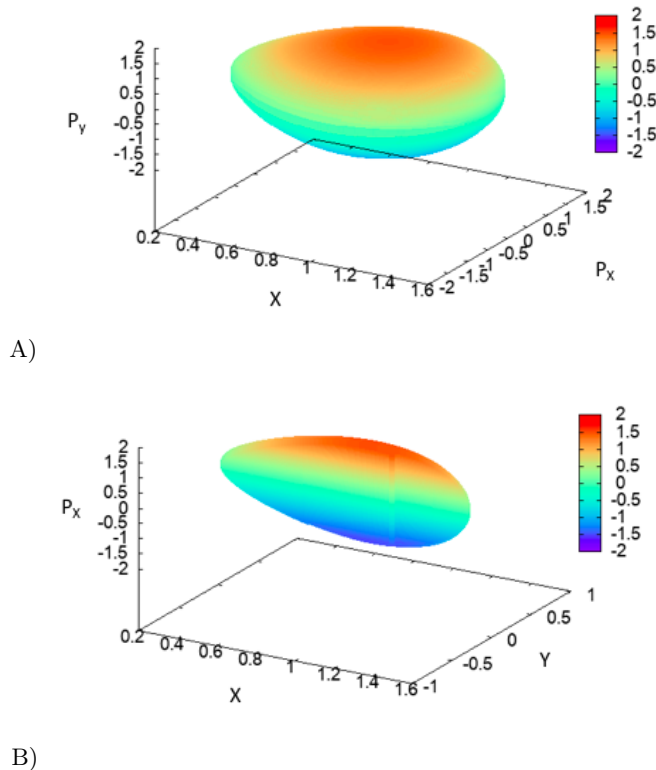
A)

B)

Figure 3. 3D projections (x, p_x, p_y) (panel A) and (x, y, p_x) (panel B) of the periodic orbit dividing surface of the family of the lower saddle for $E = -0.2$.

panel C we show that the minimum of the family of the lower saddle is always zero whilst the minimum of the top family is increasing and the minimum of the bottom family is decreasing. The same happens in the panel D for the maximum.

3. **The range of the dividing surfaces:** In Figure 7 we illustrate the range of the x coordinate, y coordinate and p_x coordinate (panels A, B and C, respectively) of the dividing surfaces of the family of the lower saddle (black line), top family (red line) and bottom family (green line), respectively. Note that we did not present the range of p_y coordinate because it is determined from the other three coordinates through the Hamiltonian of the system. In the panels A, B and C the range of the coordinates of the top family coincide with the range of the same coordinates of the bottom family. Moreover the range of the y coordinate of the family of the lower saddle is zero for all energies (see panel B). Finally, the continuation of the range of the p_x coordinate of the families is evident as the energy varies (see panel C).

V.   CONCLUSIONS

We studied a bifurcation of periodic orbit dividing surfaces that occurs because of a pitchfork bifurcation of periodic orbits in a nonlinear Hamiltonian system with two degrees of freedom. We investigated the structure, the range and the minimum and maximum of the periodic orbit dividing surfaces of the family of periodic orbits of the lower saddle of our system and of its bifurcating families of periodic orbits. Our main conclusions are:

1. The dividing surfaces of the family of periodic orbits of the lower saddle are presented as ellipsoids and filamentary structures in the 3D subspaces of the phase space. The ellipsoids become sharper as we increase the energy.

2. The dividing surfaces of the bifurcating families are presented as ellipsoids with a sharp edge or as curved filamentary structures. The sharpness of the ellipsoids decreases as we increase the energy.
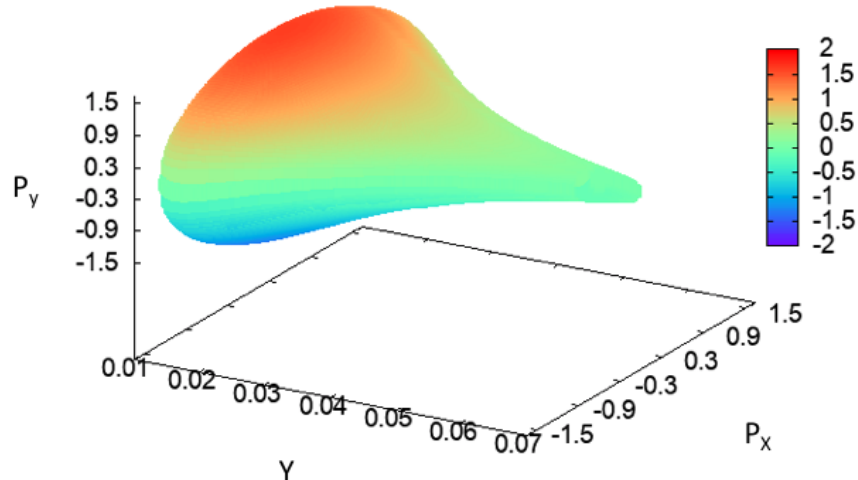
Figure 4. 3D projection (x, p_x, p_y) of the dividing surface that is constructed by the family of the top unstable periodic orbits for $E = -0.00055$.

3. The dividing surfaces of the bifurcating families coincide with the dividing surfaces of the family of the lower saddle in the (x, p_x, p_y) subspace of the phase space.

4. The dividing surfaces of the bifurcating families are on both sides of the dividing surfaces of the family of the lower saddle in the 3D subspaces of the phase space (x, y, p_x), (x, y, p_y) and (y, p_x, p_y). This happens until the disappearance of the dividing surfaces of the family of lower saddles for values of energy from 0 (for which we have the appearance of the high energy saddle) and above. As we increase the energy, the dividing surfaces of the bifurcating families move away from each other.

5. The ranges of the dividing surfaces of the bifurcating families coincide with each other and they follow the evolution of the range of the dividing surfaces of the lower saddle (except the range in the y coordinate where the range of the dividing surfaces of the lower saddle is 0).

6. The minimum and the maximum of the dividing surfaces coincide with each other with respect to the x and p_x coordinate (the p_y coordinate is determined through the Hamiltonian of the system) and they follow, in these cases, the evolution of the minimum and maximum of the dividing surfaces of the lower saddles.
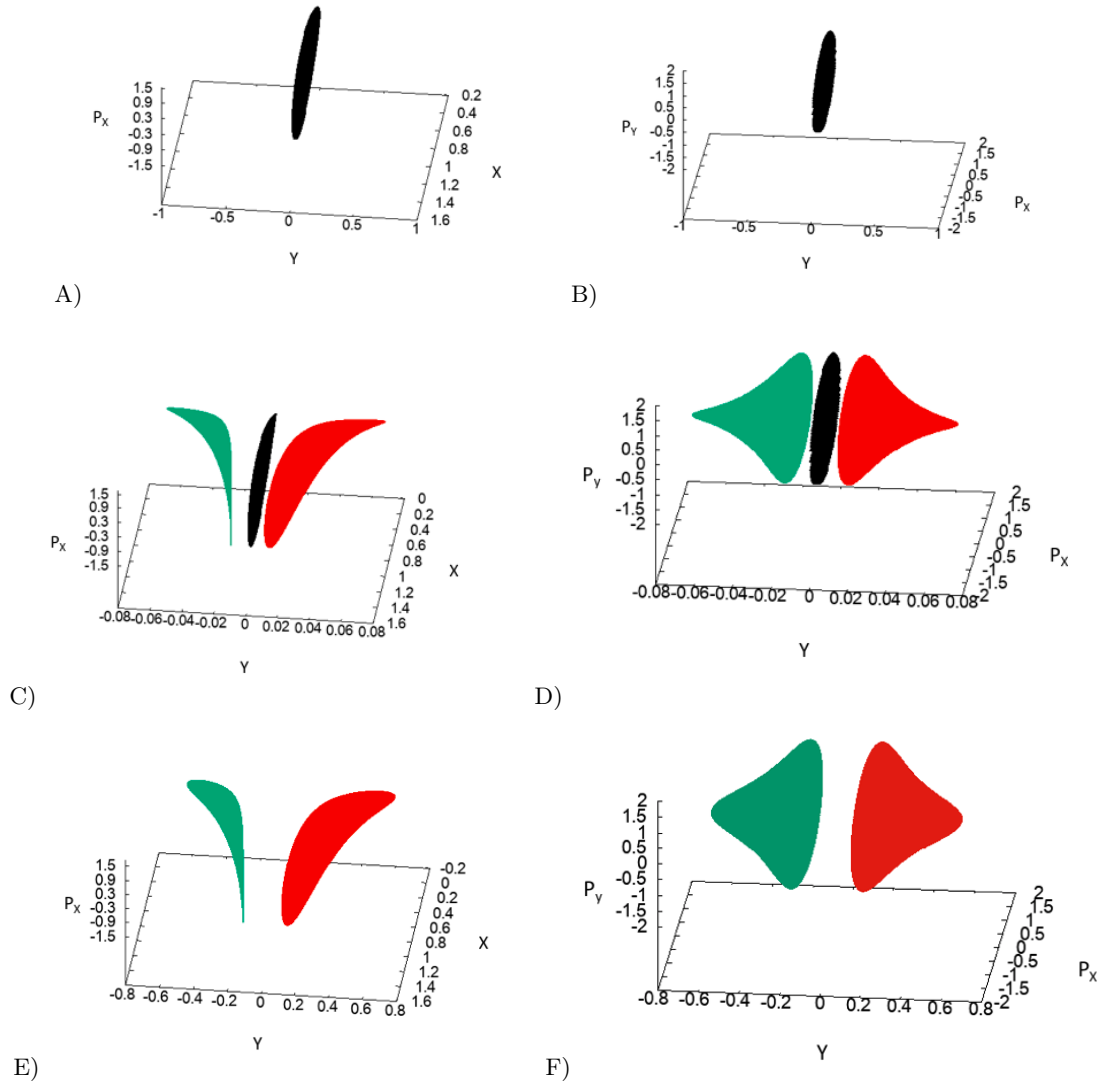
ACKNOWLEDGMENTS

Figure 5. 3D projections (x, y, p_x) (left column of the panels) and (y, p_x, p_y) (right column of the panels) of the periodic orbit dividing surface of the family of the lower saddle (with black color) and of the dividing surfaces that are constructed from the periodic orbits of the top (with red color) and bottom (with green color) unstable periodic orbits for $E = -0.2$ (first row), $E = -0.00055$ (second row) and $E = 0.2$ (third row). We encountered the same structures, as these in the 3D subspace (x, y, p_x), in the 3D subspace (x, y, p_y).
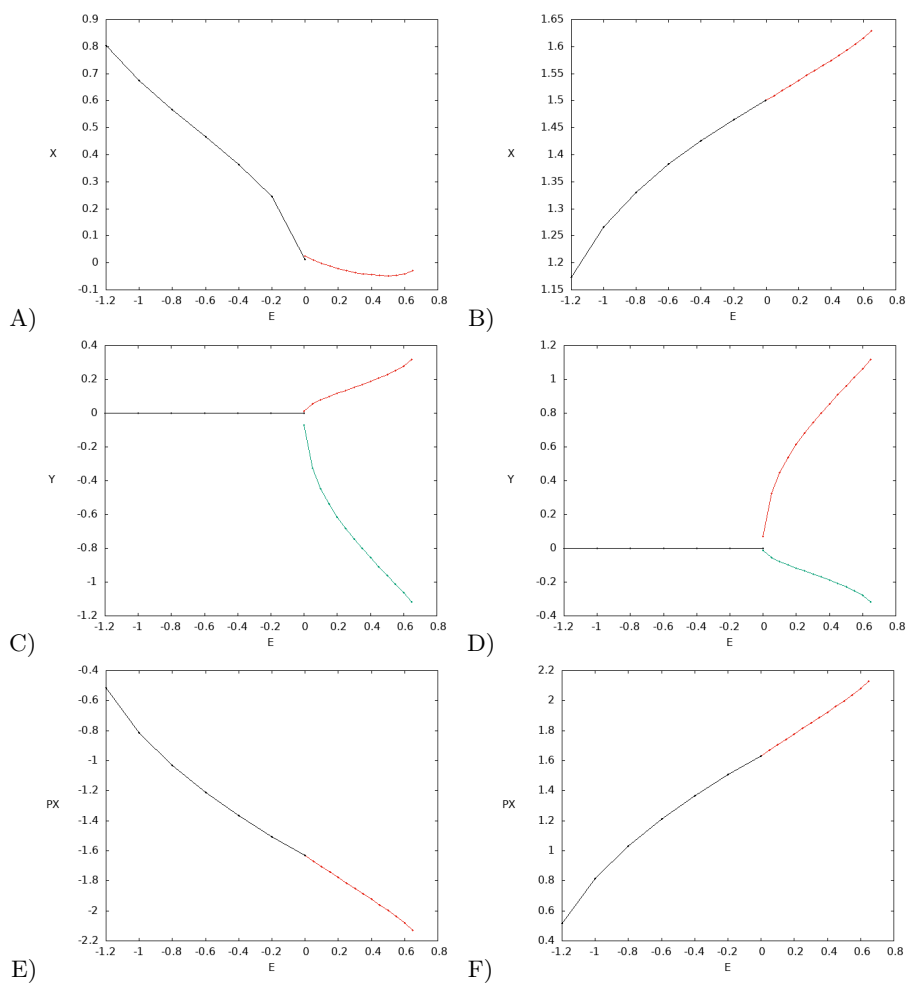
Figure 6. Diagrams for the A) mininum and B) maximum of the X coordinate of the central (black), top (red) and bottom (green) families versus the energy, C) mininum and D) maximum of the y coordinate of the central, top and bottom families versus the energy and E) mininum and F) maximum of the PX coordinate of the central, top and bottom families versus the energy.
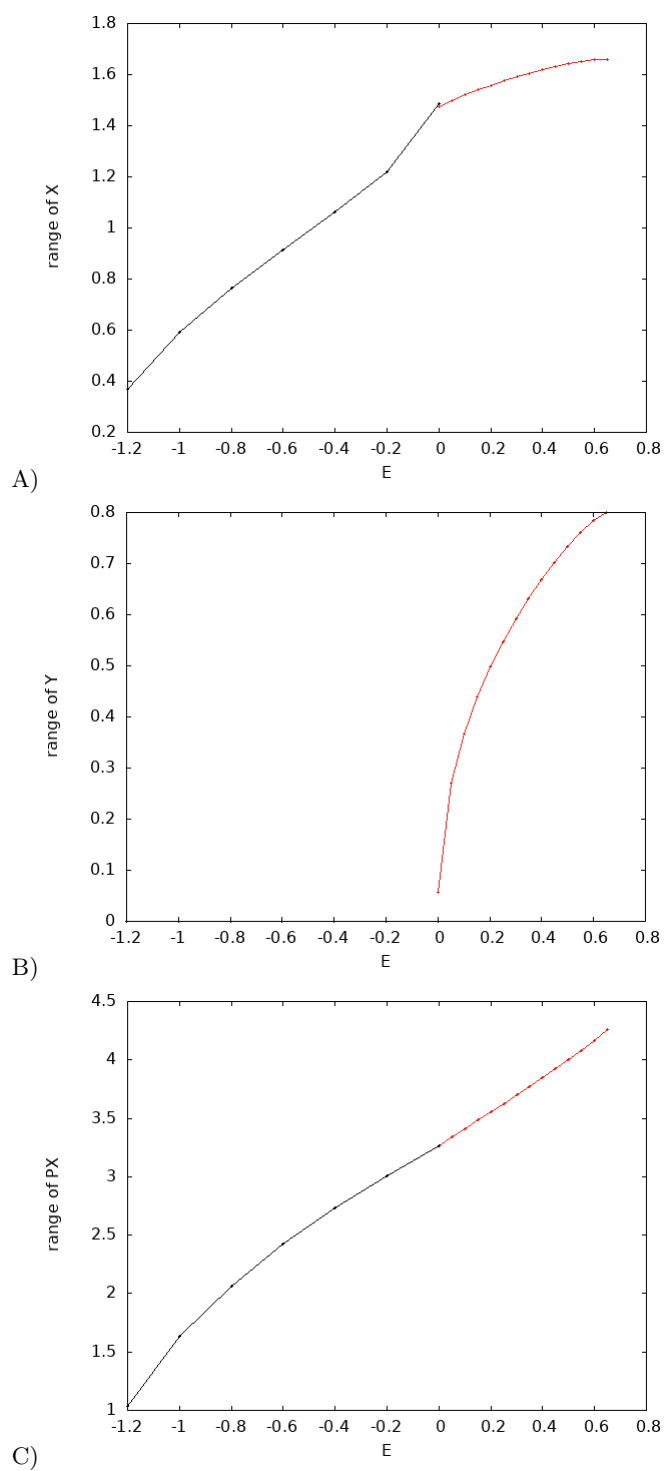
Figure 7. A) Range of the X coordinate of the central family (black line), top family (red line) and bottom family (green line) versus the energy, B) Range of the Y coordinate of the central family (black line), top family (red line) and bottom family (green line) versus the energy and C) Range of the PX coordinate of the central family (black line), top family (red line) and bottom family (green line) versus the energy
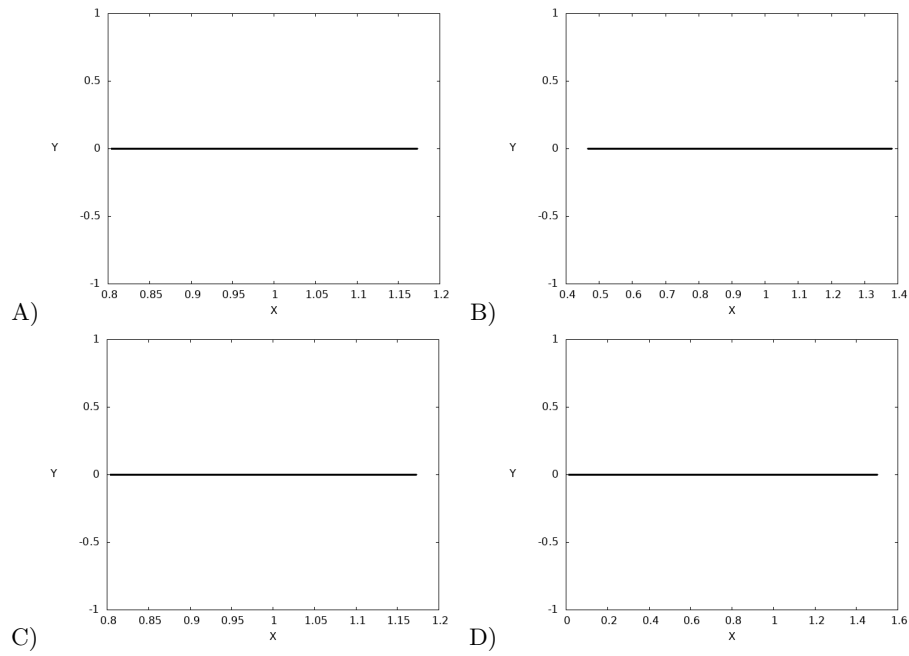
Figure 8. 2D projections of the periodic orbits of the central family in the configuration space for energies A) -1.2, B) -0.6, C) -0.2 and D) -0.00055
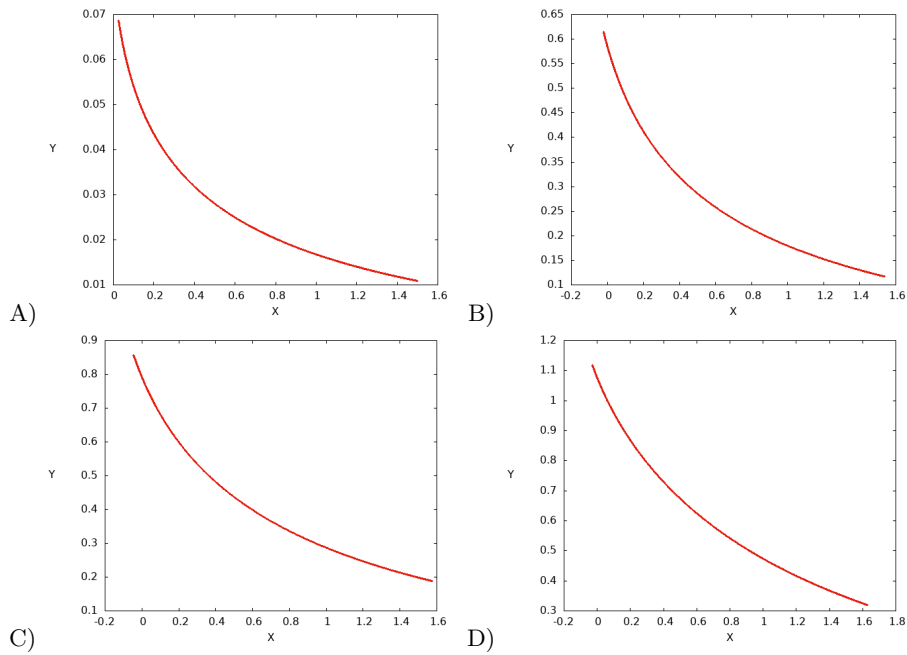
Figure 9. 2D projections of the periodic orbits of the top family in the configuration space for energies A) -0.00055, B) 0.2, C) 0.4 and D) 0.65
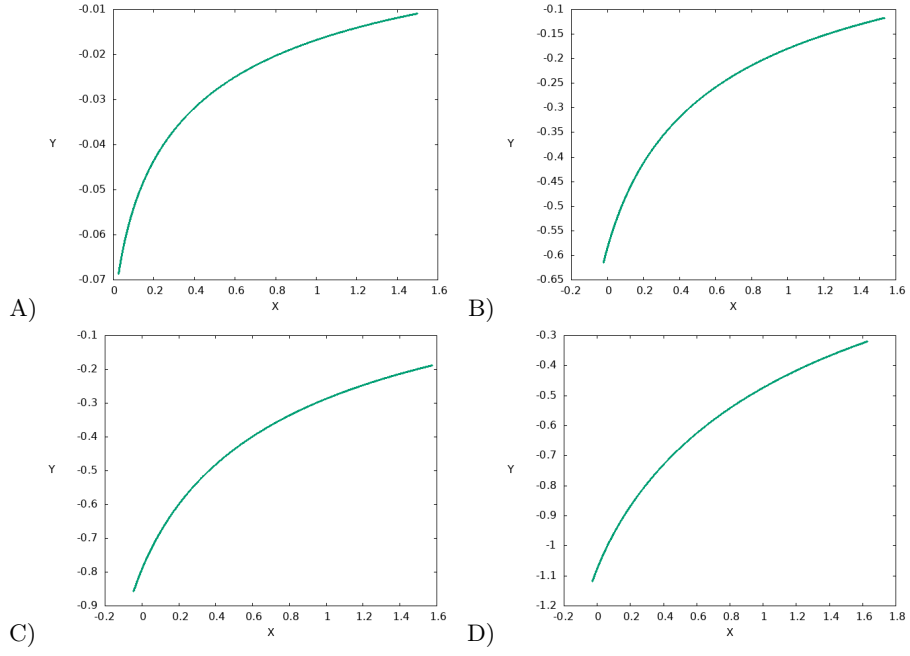
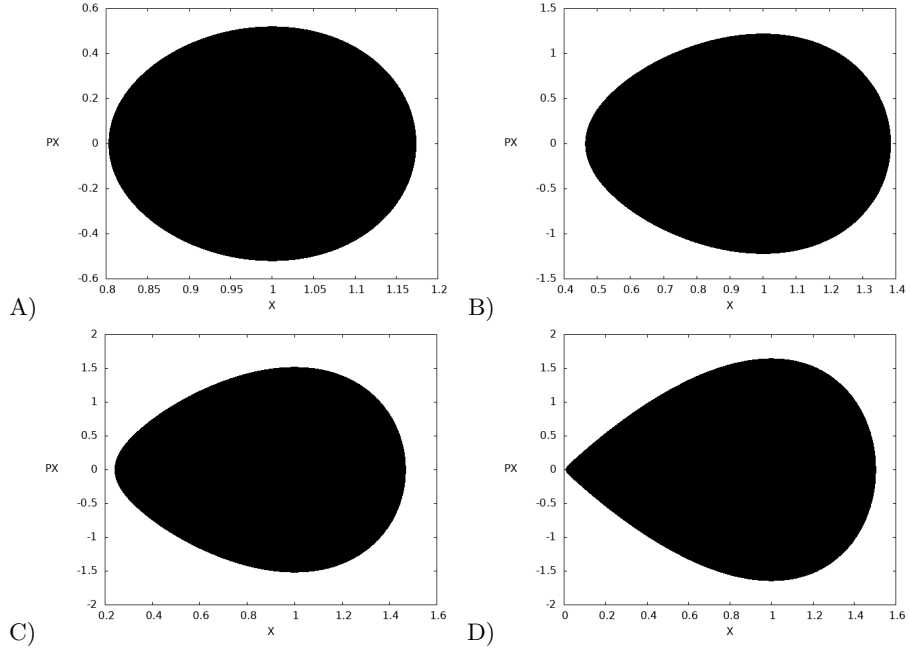Figure 10. 2D projections of the periodic orbits of the bottom family in the configuration space for energies A) −0.00055, B) 0.2, C) 0.4 and D) 0.65

Figure 11. 2D projections of the dividing surfaces of the central family in the X-PX space for energies A) −1.2, B) −0.6, C) −0.2 and D) −0.00055

Figure 12. 2D projections of the dividing surfaces of the top family in the X-PX space for energies A) −0.00055, B) 0.2, C) 0.4 and D) 0.65

Figure 13. 2D projections of the dividing surfaces of the bottom family in the X-PX space for energies A) −0.00055, B) 0.2, C) 0.4 and D) 0.65

Figure 14. 2D projections of the dividing surfaces of the central family in the Y-PY space for energies A) -1.2, B) -0.6, C) -0.2 and D) -0.00055
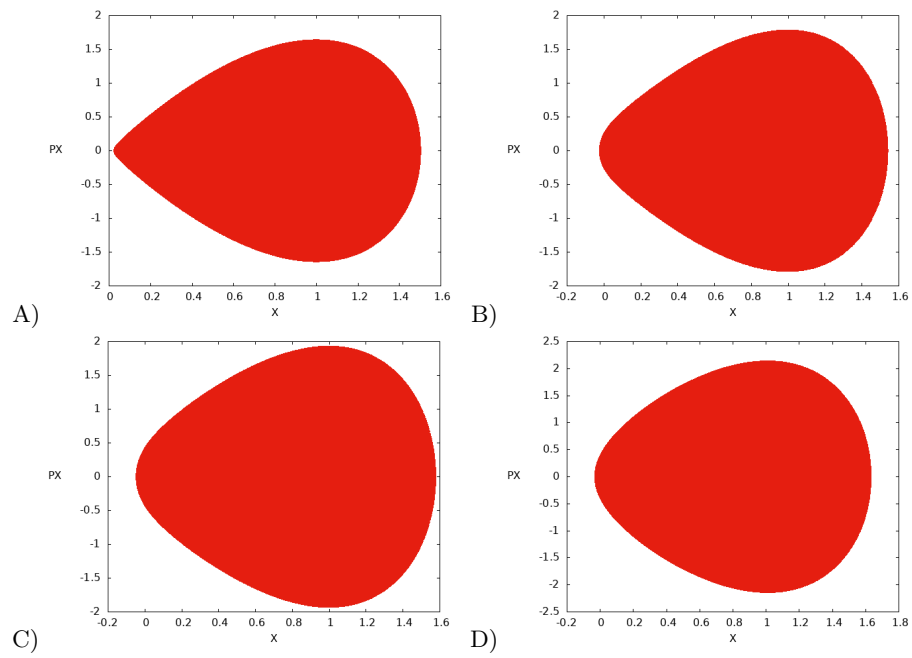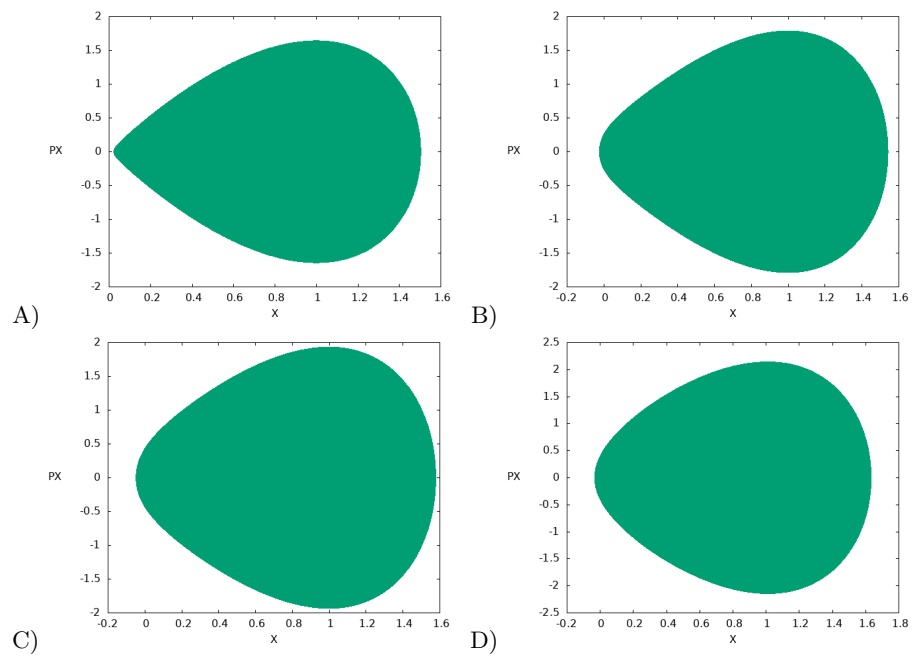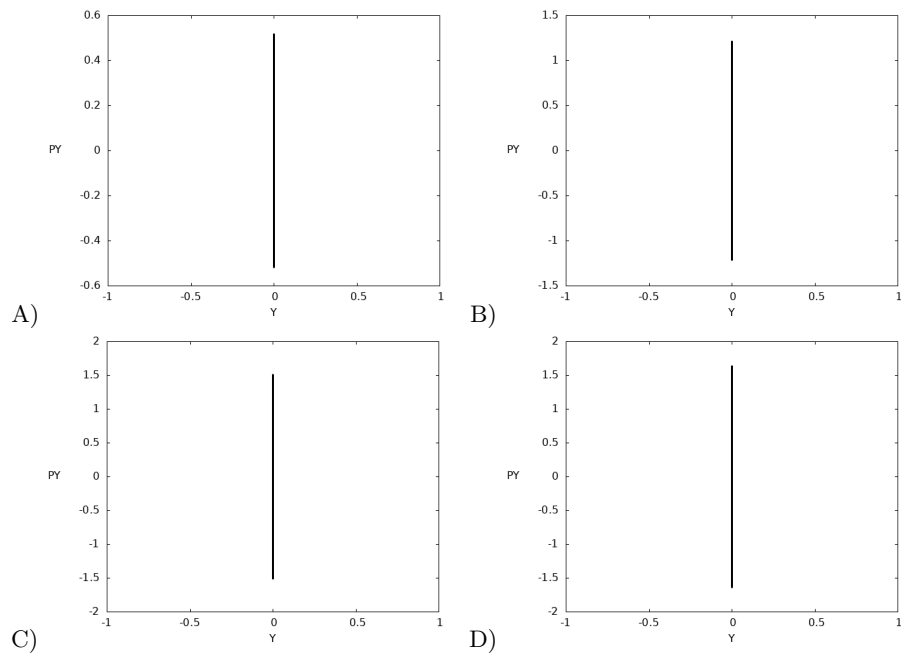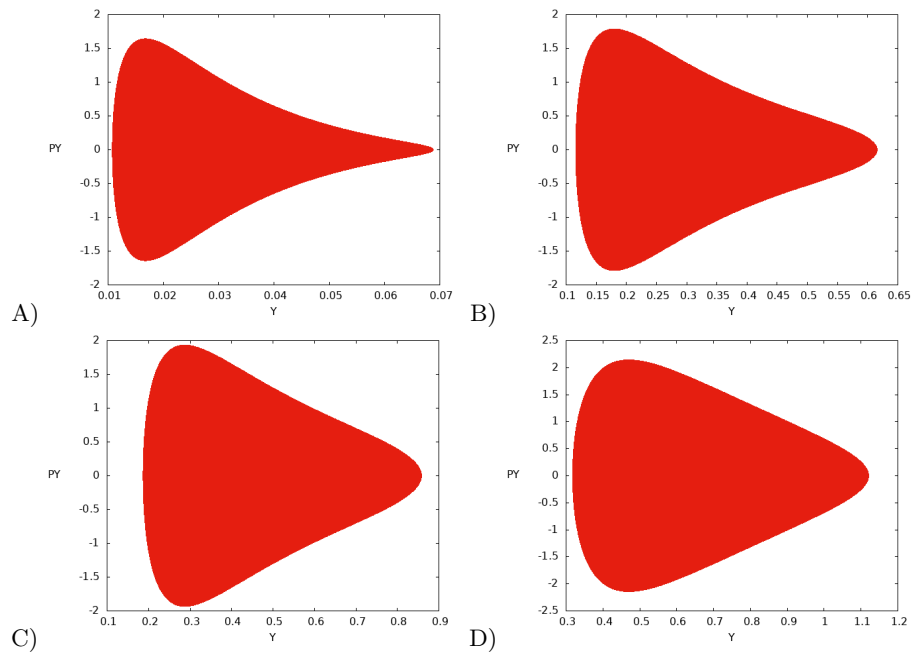

Figure 15. 2D projections of the dividing surfaces of the top family in the Y-PY space for energies A) -0.00055, B) 0.2, C) 0.4 and D) 0.65

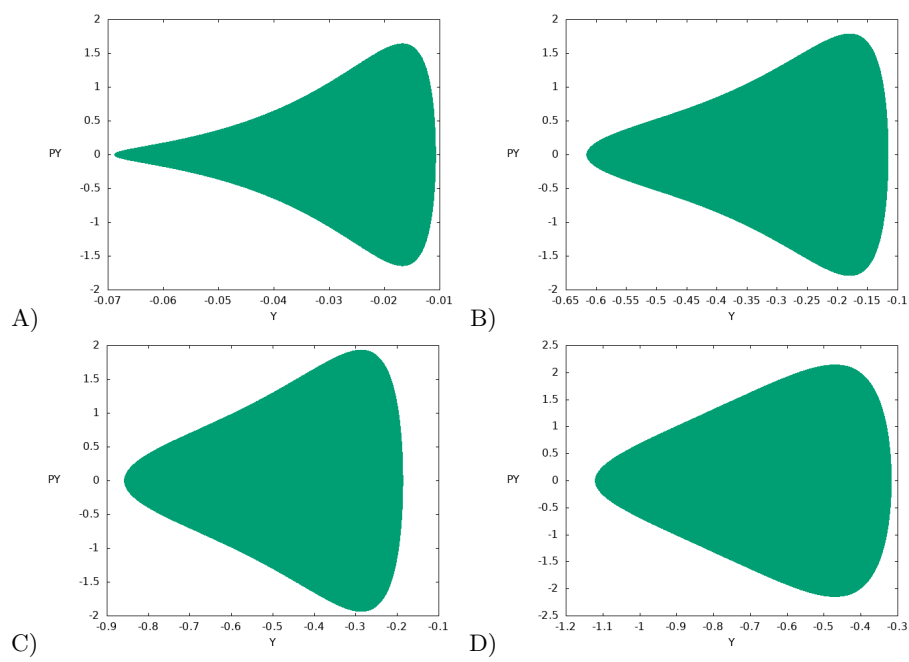Figure 16. 2D projections of the dividing surfaces of the bottom family in the Y-PY space for energies A) −0.00055, B) 0.2, C) 0.4 and D) 0.65

[1] P. Collins, B. K. Carpenter, G. S. Ezra, and S. Wiggins, Nonstatistical dynamics on potentials exhibiting reaction path bifurcations and valley-ridge inflection points, The Journal of Chemical Physics **139**, 154108 (2013).

[2] M. Katsanikas, V. J. García-Garrido, M. Agaoglou, and S. Wiggins, Phase space analysis of the dynamics on a potential energy surface with an entrance channel and two potential wells, Physical Review E **102**, 012215 (2020).

[3] M. Agaoglou, V. J. García-Garrido, M. Katsanikas, and S. Wiggins, The phase space mechanism for selectivity in a symmetric potential energy surface with a post-transition-state bifurcation, Chemical Physics Letters **754**, 137610 (2020).

[4] V. García-Garrido, M. Katsanikas, M. Agaoglou, and S. Wiggins, Tuning the branching ratio in a symmetric potential energy surface with a post-transition state bifurcation using external time dependence, Chemical Physics Letters **754**, 137714 (2020).

[5] M. Agaoglou, M. Katsanikas, and S. Wiggins, The influence of a parameter that controls the asymmetry of a potential energy surface with an entrance channel and two potential wells, Regular and Chaotic Dynamics , (was submitted) (2021).

[6] H. Douglas, M. Katsanikas, M. Agaoglou, and S. Wiggins, The time evolution of the trajectories after the selectivity in a symmetric potential energy surface with a post-transition-state bifurcation, Regular and Chaotic Dynamics , (was submitted) (2021).

[7] R. Crossley, M. Agaoglou, M. Katsanikas, and S. Wiggins, From Poincaré maps to Lagrangian descriptors: The case of the valley ridge inflection point potential, Regular and Chaotic Dynamics **26**, 147 (2021).

[8] E. Wigner, The transition state method, Transactions of the Faraday Society **34**, 29 (1938).

[9] H. Waalkens, R. Schubert, and S. Wiggins, Wigner's dynamical transition state theory in phase space: classical and quantum, Nonlinearity **21**, R1 (2007).

[10] P. Pechukas and F. J. McLafferty, On transition-state theory and the classical mechanics of collinear collisions, The Journal of Chemical Physics **58**, 1622 (1973).

[11] P. Pechukas and E. Pollak, Trapped trajectories at the boundary of reactivity bands in molecular collisions, The Journal of Chemical Physics **67**, 5976 (1977).

[12] P. Pechukas and E. Pollak, Classical transition state theory is exact if the transition state is unique, The Journal of Chemical Physics **71**, 2062 (1979).

[13] E. Pollak, Periodic orbits and the theory of reactive scattering, Theory of Chemical Reaction Dynamics **3**, 123 (1985).

[14] P. Pechukas, Transition state theory, Annual Review of Physical Chemistry **32**, 159 (1981).

[15] M. Katsanikas and S. Wiggins, The generalization of the periodic orbit dividing surface for Hamiltonian systems with three or more degrees of freedom in chemical reaction dynamics - I, International Journal of Bifurcation and Chaos , in press (2021).

[16] M. Katsanikas and S. Wiggins, The generalization of the periodic orbit dividing surface for Hamiltonian systems with three or more degrees of freedom in chemical reaction dynamics - II, International Journal of Bifurcation and Chaos , in press (2021).

[17] R. S. MacKay and D. C. Strub, Bifurcations of transition states: Morse bifurcations, Nonlinearity **27**, 859 (2014).

[18] I. Burghardt and P. Gaspard, The molecular transition state: From regular to chaotic dynamics, The Journal of Physical Chemistry **99**, 2732 (1995).

[19] M. Inarrea, J. F. Palacian, A. I. Pascual, and J. P. Salas, Bifurcations of dividing surfaces in chemical reactions, J. Chem. Phys. **135**, 014110 (2011).

[20] C. B. Li, M. Toda, and T. Komatsuzaki, Bifurcation of no-return transition states in many-body chemical reactions, J. Chem. Phys. **130**, 124116 (2009).

[21] A. Allahem and T. Bartsch, Chaotic dynamics in multidimensional transition states, J. Chem. Phys. **137**, 214310 (2012).

[22] M. Founargiotakis, S. Farantos, C. Skokos, and G. Contopoulos, Bifurcation diagrams of periodic orbits for unbound molecular systems: Fh2, Chemical Physics Letters **277**, 456 (1997).

[23] F. A. Mauguiere, P. Collins, G. S. Ezra, and S. Wiggins, Bifurcations of normally hyperbolic invariant manifolds in analytically tractable models and consequences for reaction dynamics, International Journal of Bifurcation and Chaos **23**, 1330043 (2013).

[24] S. C. Farantos, R. Schinke, H. Guo, and M. Joyeux, Energy localization in molecules, bifurcation phenomena, and their spectroscopic signatures: The global view, Chemical Reviews **109**, 4248 (2009).

[25] W. Lyu, S. Naik, and S. Wiggins, Hamiltonian pitchfork bifurcation in transition across index-1 saddles, arXiv preprint arXiv:2102.10933 (2021).

[26] P. H. Rabinowitz, Periodic solutions of Hamiltonian systems: a survey, SIAM Journal on Mathematical Analysis **13**, 343 (1982).

[27] A. Weinstein, Normal modes for nonlinear Hamiltonian systems, Inventiones Mathematicae **20**, 47 (1973).

[28] J. Moser, Periodic orbits near an equilibrium and a theorem by alan weinstein, CPAM **29**, 727 (1976).

[29] E. Pollak and P. Pechukas, Transition states, trapped trajectories, and classical bound states embedded in the continuum, The Journal of Chemical Physics **69**, 1218 (1978).

[30] G. S. Ezra and S. Wiggins, Sampling phase space dividing surfaces constructed from normally hyperbolic invariant manifolds (NHIMs), The Journal of Physical Chemistry A **122**, 8354 (2018).